Journal of Geosciences, 58 (2013), 133–148 DOI: 10.3190/jgeosci.140

Original paper

Age and origin of the tourmaline-rich hydraulic breccias in the Tatra Granite, Western Carpathians

Aleksandra GAWĘDA[1*], Axel MÜLLER[2], Holly STEIN[3,4], Mariola KĄDZIOŁKO-GAWEŁ[5], Stanisław MIKULSKI[6]

[1] *Faculty of Earth Sciences, University of Silesia, Będzińska st. 60, 41-200 Sosnowiec, Poland; aleksandra.gaweda@us.edu.pl*
[2] *Geological Survey of Norway (NGU), Leiv Erikssons vei 39, 7040 Trondheim, Norway*
[3] *AIRIE Program, Colorado State University, USA*
[4] *CEED Centre of Excellence, University of Oslo, Norway*
[5] *Institute of Physics, University of Silesia, Uniwersytecka 4, 40-007 Katowice, Poland*
[6] *Polish Geological Institute, Rakowiecka 4, 00-975 Warszawa, Poland*
[*] *Corresponding author*

In the crystalline basement of the Tatra Mountains (Poland/Slovakia) two types of tourmaline-rich breccia zones are described, both having originated from magmatic fluids and showing a 350 ± 1 Ma Re–Os model age. Both T1 brecciated pegmatites and T2 vein-breccias are cemented by a tourmaline–quartz matrix. In T1 breccias, the metasomatic replacement of feldspars by tourmaline and overgrowths of small Tur_2 tourmalines on the primary pegmatitic Tur_1 tourmaline crystals suggest an important role for metasomatic processes. The microcrystalline nature of the quartz–tourmaline matrix and high vacancy ratios in the X-site in tourmaline from T2 breccias reflect relatively rapid crystallization from an oxidized fluid. The formation of both types of breccias is related to the internal structure of the Tatra granitoid intrusion. The layered character of the granitoid body probably stimulated the formation of pegmatite-like pockets, with local overpressure causing metasomatic alteration, rock brecciation and cementation by tourmaline (T1 breccias), the final hydrofracturing of overburden rocks and fluid escape. The resulting fracture zones (T2) are interpreted as the paths for fluid migration and rapid crystallization as the pressure and temperature dropped from 7.5–6 kbar and 630–570 ºC in the case of the T1 brecciated pegmatites to 2.5–1.5 kbar and 465–430 ºC in the vein T2 breccias.

Keywords: tourmaline, hydraulic breccias, Re–Os molybdenite dating, quartz chemistry, Tatra Mountains
Received: 15 February 2013; accepted: 13 June 2013; handling editor: P. Uher

1. Introduction

Tourmaline is a common accessory mineral in granitoids, especially peraluminous leucogranites and their pegmatites, formed as a result of continental collision (e.g. London 1996; Buriánek and Novák 2007; Slack and Trumbull 2011). Tourmaline crystallizes as a magmatic mineral, as a subsolidus phase and as a late hydrothermal mineral, especially at the exocontacts of granitoid plutons. The presence of tourmalines is a marker of high B activity. The chemical composition of tourmalines mirrors the character of source rocks and might help to define the origin of the boron (Henry and Guidotti 1985; van Hinsberg et al. 2011a, b).

Boron in granitic magma, especially in combination with phosphorus and fluorine, increases dramatically the solubility of H_2O, and reduces melt viscosity. This results in enhanced partitioning of B into the fluid phase, the enhanced solubility of silica in the fluid phase and high hydrostatic pressure during final crystallization (Pollard et al. 1987; London 2009). Boron-rich fluids, released from the crystallizing granitoid magma, circulate in the contact aureoles and cause metasomatic reactions (tourmalinization and silicification) and/or hydrofracturing in both the granite and the host rocks (Müller and Halls 2005; Dini et al. 2008; Slack and Trumbull 2011). When the internal pressure of the fluids exceeds the lithostatic one, the hydrofracturing triggers a breccia pipe and stockwork formation, both mineralized with Cu, Au, Mo, Zn and Sn ores and barren types, in the apical parts of granitic bodies (Derham and Feely 1988; Williamson et al. 2000; Skewes et al 2003; Dini et al. 2008; Feely et al. 2010). In the zones of hydrofracturing the solid rocks are fragmented and cemented by minerals crystallizing from the exsolved fluid, forming tourmaline-bearing breccias (Skewes et al. 2003; Müller and Halls 2005; Dini et al. 2008). Metasomatic reactions are commonly developed, depending on the partial pressure of the fluid components and depth of granite pluton emplacement. Two models for the generation of such breccias are proposed:

1. explosive hydrothermal brecciation ("burst breccias"), a result of the exsolution of superheated late-magmatic fluids, migrating as jets of steam and fracturing the

overlying rocks close to the surface (Skewes et al. 2003; Dini et al. 2008 and references therein);
2. hydrothermal collapse brecciation, formed by the metasomatic action of hydrothermal fluids (Sillitoe and Sawkins 1971).

Tourmaline that may be related to the ore mineralization, usually pre- or post-dates it, and spatial relations can be misleading (Slack and Trumbull 2011). Increasing B concentrations in the magma promote increasing metal solubility due to increasing H_2O solubility, although B is not directly involved in the transport and concentration of metals (Müller et al. 2006). However, tourmaline mirrors the fluid composition and its redox state, which can be a trigger for ore deposition. The oxidation state of the fluid is recorded by Fe^{3+}/Fe^{2+} variations in the tourmaline structure (Fuchs et al. 1998; Pieczka and Kraczka 2004). Tourmaline precipitating as a secondary mineral in shear or fracture zones shows usually a rather narrow compositional range, due to a high fluid flux and relatively rapid precipitation.

The presence of tourmaline-rich, molybdenite-bearing hydraulic breccias cutting the layered structures of the granitoid intrusion, provides an excellent opportunity to study the fate of the boron-rich, granite-derived fluid and the age of the mineralization. The aim of this paper is to describe the zones of fracturing, mineralized predominantly by tourmaline and quartz, with locally dispersed molybdenite, found at several locations in the Tatra Mts. crystalline core, but always spatially connected with the presence of layering in the granites. The origin and age of the mineralization found in these zones and their relationship to the internal structure of the Tatra intrusion is also discussed. Although the temperature range of tourmaline crystallization under post-magmatic conditions is relatively wide (550–150 ºC; Müller et al. 2005; Slack and Trumbull 2011), the rapid crystallization of breccias and the presence of rutile coexisting with quartz allowed the application of the Ti-in-quartz geothermometer of Wark and Watson (2006) to co-precipitating quartz and tourmaline and, lastly, a P–T path determination.

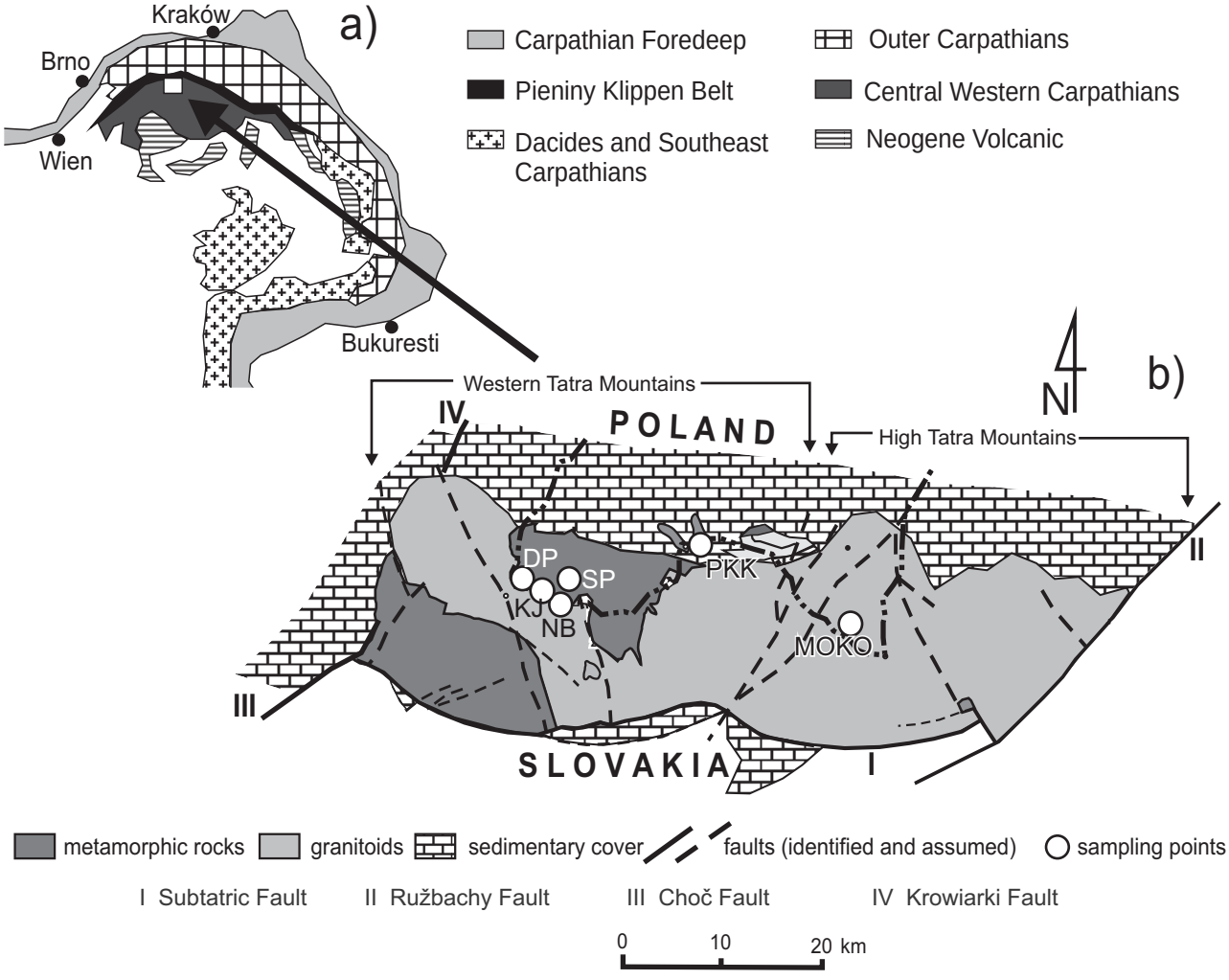

Fig. 1 The geology of the Tatra Mountains. **a** – Simplified geological sketch of the Carpathian chain; **b –** Simplified geological map of the Tatra Mountains block (after Gawęda 2009) with marked sampling points.

2. Geological setting

The Tatra Massif is one of the crystalline units within the Inner Western Carpathians (Fig. 1a). The crystalline basement of the Tatra Mountains is built of the polygenetic Variscan Tatra intrusion and its metamorphic envelope (Fig. 1b). The crystalline complex is covered by nappes of Mesozoic sedimentary formations (Fig. 1b). The present-day structure of the Tatra Massif is a result of Paleogene uplift and division of the whole massif into small tectonic blocks at 36–24 to *c.* 10 Ma (Burchart 1972; Kohút and Sherlock 2003) and final tilting to the north at *c.* 30 degrees along the Sub-Tatric Fault (Fig. 1b; Grabowski and Gawęda 1999).

Metamorphic rocks are preserved mostly in the western part of the massif, the Western Tatra Mountains (Fig. 1b) and were intensively migmatized at *c.* 360 Ma (Burda and Gawęda 2009). Inside the Western Tatra metamorphic envelope, tourmaline-bearing pegmatites are present. They are thought to be associated with the evolution of anatectic melt and have been dated at 345 ± 9.5 Ma by the WR Rb–Sr method (Gawęda 1995). The schorl–dravite series tourmaline crystallization in the pegmatites reflects boron and water activity, variable oxygen fugacity and restricted Fe–Mg mobilization during anatexis and pegmatite fluid fractionation (Gawęda et al. 2002).

The tongue-shaped Tatra granitoid intrusion (Kohút and Janák 1994) consists of several magmatic pulses, all dated by the U–Pb method on zircon: I-type mingled hybrid quartz diorite, interpreted as a mafic precursor and dated at 368 ± 8 Ma, tonalite–granodiorite showing an age interval of 360–370 Ma, syenogranite–monzogranite, locally porphyritic, rich in xenoliths and mafic microgranular enclaves, dated from 350 ± 5 Ma to 337 ± 6 Ma (Poller et al. 2000; Gawęda et al. 2005; Gawęda 2008, 2009; Burda et al. 2011, 2013). Formerly, these granites were dated at 314 ± 4 Ma (Poller and Todt 2000) but this age was later interpreted as to be influenced by the Pb-loss caused by post-magmatic shearing (Gawęda 2009).

The granitoid intrusion shows internal layering, formed as a result of mixing of mafic and felsic magma batches during flow (Burda et al. 2011; Gawęda and Szopa 2011). The formation of sedimentary-like structures in the granite was facilitated by the high content of volatiles, including H_2O, B, CO_2, P_2O_5, and locally CH_4 (Gawęda and Szopa 2011; Szopa et al. in print). As the layering shows normal density gradation and inverse size gradation, the bottoms of layers are enriched in mafic minerals whilst the tops are felsic and sharply bordered by the mafic bottoms of the overlying layer (Fig. 2a). Locally, the pegmatite-like lenses are concentrated in the felsic part of the layer (Fig. 2b).

3. Sample description

Two types of tourmaline-bearing breccias were identified in the field, all associated with layered granitoids.

Pegmatite-like pockets and pseudo-layers (T1) are up to 20 cm thick and show the internal brecciation. The pegmatite-like pockets, typically with graphic texture, are located on the top of the graded layers (Figs 2a–b and figures in Gawęda and Szopa 2011), and sporadically grade into T1 breccia zones.

Their presence is also correlated with partially molten metapelitic xenoliths (Pawlica 1913; Gawęda 2009). When tourmaline is lacking in the pegmatite-like pockets, brecciation is not observed (compare Fig. 2b–c). In T1 brecciated pegmatites (Fig. 2c) the primary tourmalines Tur_1 are overgrown by secondary Tur_2 fine-grained types (Fig. 3a), whilst primary K-feldspars show partial metasomatic replacement by Tur_2 tourmaline (Fig. 3b).

The tourmaline-rich breccia veins are 2–3 metres long and 6–20 cm wide, anastomosing into millimetre-thick veins, trending 20–40° to SSE, cutting discordantly layered and non-layered granitoids (Fig. 2d–e).

Both types of breccias are cemented by fine-grained to submicroscopic tourmaline, quartz, feldspars and muscovite (Fig. 3c–d, f). Quartz crystals are closely intergrown with tourmaline showing blue–dark blue to khaki–grey pleochroism, minute K-feldspar and albite. Prismatic and needle-shaped rutile is rarely observed in quartz. Xenomorphic to subidiomorphic fluorapatite is locally intergrown with tourmalines (Fig. 3d). Fine-grained zoned phengitic muscovite occurs as an accessory mineral in T1 breccias (Tab. 1; Fig. 3e), whilst in T2 breccias unzoned phengitic muscovite flakes are present (Tab. 1; Fig. 3f). Submicroscopic sulphides (molybdenite, tetrahedrite or pyrite) are sporadically found (e.g. Wątocki 1950; Gawęda et al. 2007). In one case a molybdenite crystal reaching 6 mm in diameter was observed (Fig. 2e).

Field observations at the contact of the crystalline core and Mesozoic sedimentary cover of the Tatra Mountains preclude an Alpine age for the tourmaline-rich breccias: they cut discordantly the crystalline rocks (e.g. Fig. 2d; PKK sample) but do not continue into the sedimentary cover.

4. Analytical methods

The analyses of tourmalines and associated minerals were carried out on CAMECA SX-100 electron microprobe in the Inter-Institution Laboratory of Microanalysis of Minerals and Synthetic Substances in Warsaw, using sets of natural and synthetic standards. Microanalyses were carried out at 15 kV and 10 nA, with counting times of 20 s for all elements, except boron. The amount of B_2O_3 was calculated from stoichiometry, assuming three boron

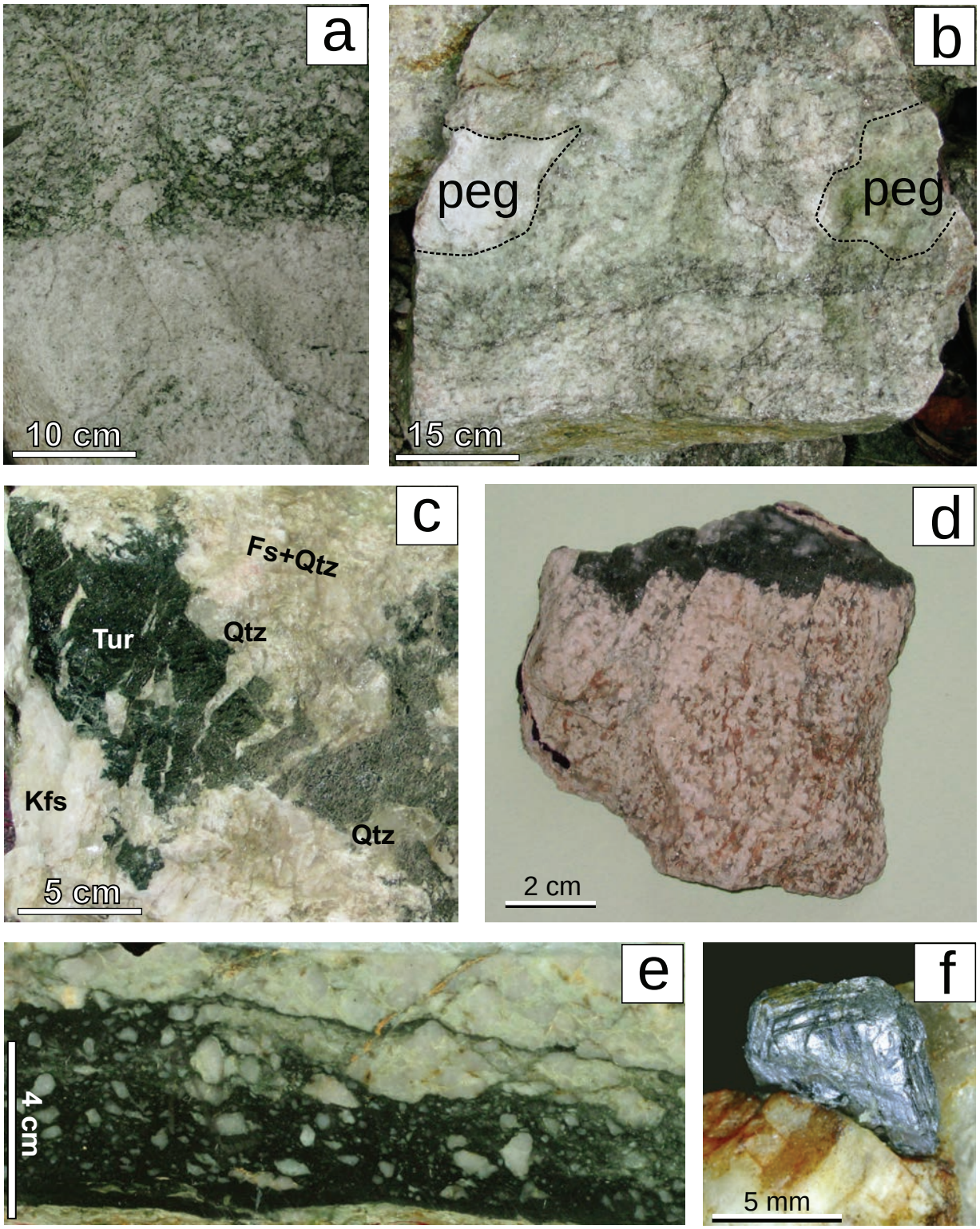

Fig. 2 Textures and mineralogy of host rocks and hydraulic tourmaline-rich breccias: **a –** A fragment of the magmatic layering from the High Tatra Mountains: a contact of the felsic upper part of the underlying layer screened by the mafic (biotite-rich) base of the overlying one; **b –** Position of the pegmatite-like (in this case tourmaline-free) segregation in a single layer; **c –** Brecciated tourmaline-rich segregation (MOKO sample), as an example of the T1 breccia type; **d –** T2 breccia inside the leucogranite (PKK sample) with tourmaline and quartz-dominated matrix **e –** T2 breccia inside the granite (NB sample) showing a cataclastic fabric; the dark filling is composed predominantly of microcrystalline tourmaline; **f –** Largest molybdenite crystal, used for dating and S isotope analysis (DP sample). Abbreviations used: peg – pegmatite-like segregation; Tur – tourmaline, Qtz – quartz, Kfs – K-feldspar.

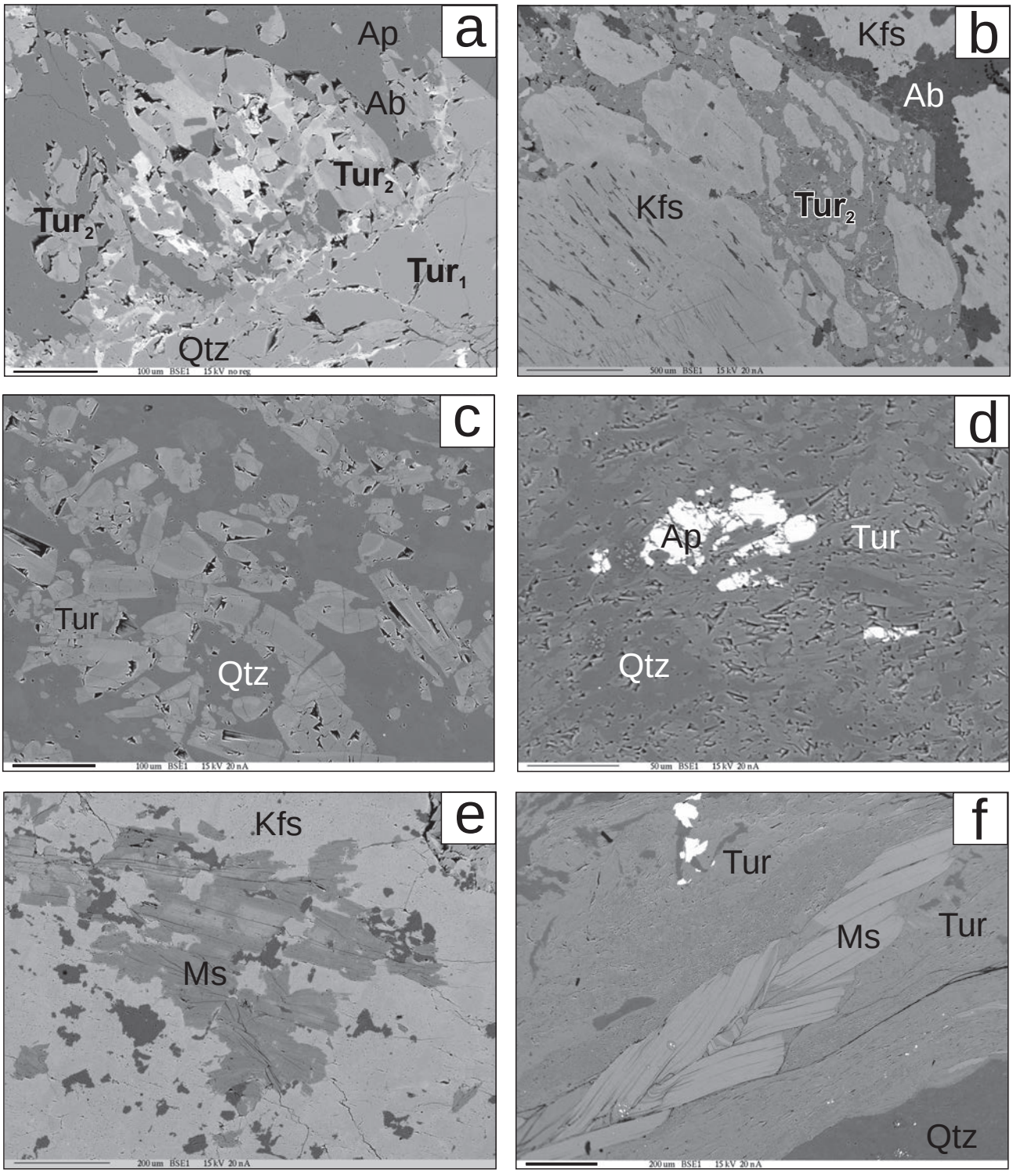

Fig. 3 Back-scattered electron (BSE) images of the matrix of hydraulic breccias from the Tatra Mts: **a** – Secondary tourmaline (Tur_2) overgrowing primary one (Tur_1) in brecciated MOKO pegmatite (T1 breccia); **b** – Replacement of K-feldspar by tourmaline in brecciated MOKO pegmatite (T2 breccia); idiomorphic shape of primary K-feldspar is still preserved; **c** – Zoned tourmaline crystals intergrown with quartz from the PKK sample (T2 breccia); **d** – Unzoned tourmaline micro-crystals intergrown with quartz and apatite (Ap) from KJ sample (T2 breccia); **e** – Zoned muscovite (Ms) in the Kfs crystal of brecciated MOKO sample (T1 breccia); **f** – Unzoned syntectonic muscovite in the tourmaline-rich microcrystalline matrix, SP sample (T2 breccia).

Tab. 1 Chemical composition and crystal-chemical formulae of muscovite from T1 and T2 breccias

Sample	T1 - pegmatite		T2 breccia		
Component	Ms-1	Ms-2	Ms-3	Ms-4	Ms-5
SiO_2	48.47	48.61	45.77	46.91	45.95
TiO_2	0.27	0.05	0.40	0.04	0.31
Al_2O_3	30.83	32.06	33.06	35.62	34.75
Cr_2O_3	0.00	0.00	0.02	0.00	0.00
FeO	2.83	2.15	4.07	0.72	2.85
MnO	0.00	0.11	0.05	0.08	0.05
MgO	2.28	2.18	0.80	0.74	0.70
CaO	0.02	0.00	0.00	0.00	0.00
BaO	0.49	0.11	0.00	0.30	0.00
Na_2O	0.14	0.15	0.56	0.43	0.81
K_2O	10.87	10.58	10.46	11.05	10.66
Total	96.20	96.00	95.19	95.89	96.08
Si	6.460	6.355	6.198	6.209	6.128
Al^{IV}	1.540	1.645	1.802	1.791	1.872
Al^{VI}	3.302	3.303	3.473	3.766	3.590
Ti	0.027	0.005	0.040	0.003	0.031
Cr	0.000	0.000	0.002	0.000	0.000
Fe^{+3}	0.199	0.286	0.290	0.050	0.200
Fe^{+2}	0.117	0.168	0.171	0.029	0.118
Mn	0.000	0.012	0.006	0.009	0.006
Mg	0.453	0.350	0.162	0.147	0.138
Ca	0.002	0.000	0.000	0.000	0.000
Ba	0.026	0.005	0.000	0.016	0.000
Na	0.035	0.039	0.148	0.111	0.209
K	1.848	1.765	1.807	1.866	1.815
#fm	0.205	0.324	0.513	0.165	0.461

#fm = $Fe^{2+}/(Fe^{2+} + Mg)$
Fluorine was below the detection limit of 0.02 wt. %

cations in the crystal-chemical formula, as well as water content (e.g. Henry et al., 2011). The following standards and K_α X-ray lines were used: albite (Na), orthoclase (K), wollastonite (Ca), corundum (Al), diopside (Mg, Si), rutile (Ti), hematite (Fe), rhodonite (Mn), synthetic phlogopite (F), and synthetic Cr_2O_3 (Cr). The crystal-chemical formulae were recalculated for 31 (O,OH,F) a.p.f.u. according to the general scheme: $XY_3Z_6T_6O_{18}(BO_3)_3V_3W$, where: X = Na, Ca, K, Cs, vacancies (V), Y = Fe, Mg, Mn, Ti, Al, Z = Al, T = Si, Al, B = B, $V + W$ = OH + F = 4. Site occupancies were calculated assuming that Si deficiency in the tetrahedral site (T) is compensated by Al. Consequently, if Al < 6, Ti, Fe^{3+} and Mg compensate Z-site occupancy (Hawthorne et al. 1993; Ertl et al. 2012), while octahedral site (Y) is filled by the remaining Al, Mg, Mn, Fe^{2+}, Fe^{3+} and $Fe^{2.5+}$ cations (Pieczka and Kraczka 2004). The X site is occupied by Na, Ca or may be vacant (MacDonald et al. 1993; von Goerne et al. 2011). The OH content in a.p.f.u. was assessed by charge balance. The tourmaline classification scheme of Henry et al. (2011) was applied.

Mössbauer absorption spectra for one selected monomineralic tourmaline and one muscovite sample from the hydrofracturing zone were recorded at room temperature using a constant acceleration spectrometer with a 57Co:Pd source. Metallic iron powder (α-Fe) absorber was used for velocity and isomer shift calibration of the Mössbauer spectrometer in the Physics Department of the University of Silesia.

A single sample of well-developed molybdenite was used for age determination according to procedure of Stein et al. (2001). Thirty milligrams of molybdenite were separated using a small hand held drill. The AIRIE Program uses an occurrence-driven strategy for Re–Os dating, which means that robust age results are not dependent on a milligram quantity of molybdenite (see Stein 2006).

The sulphur isotope composition of the same molybdenite was determined using the Delta 5 Thermo Finnigan mass-spectrometer at the Laboratory of Isotope Geology and Geo-Ecology of Wrocław University, Poland. The following isotopic standards were used: barium sulphide (Atlantic Ocean with $\delta^{34}S_{CDT}$ = –20.06 ‰ in relation to V-CDT; $\delta^{18}O_{SMOW}$ = –9.91 ‰ in relation to V-SMOW) *IAEA-S-1* ($\delta^{34}S_{CDT}$ = –0.3 ‰ in relation to V-CDT), *IAEA-SO-5* ($\delta^{34}S_{CDT}$ = +0.5 ‰ in relation to V-CDT) and *IAEA-SO-6* ($\delta^{34}S_{CDT}$ = –34.1 ‰ in relation to V-CDT). The measurement error (2σ) for $\delta^{34}S$ was below +0.3 ‰.

Laser ablation inductively coupled plasma mass spectrometer (LA-ICP-MS) at the Geological Survey of Norway, Trondheim was used to determine trace-element contents in quartz associated with tourmaline. It is a double focusing sector field instrument (ELEMENT-1 Finnigan MAT) combined with a New Wave UP-193 nm excimer laser probe. Continuous raster ablation was carried out, resulting in ablated rasters of approximately 150×100 nm with depths of 20 to 30 μm. Element concentrations were calculated by multi-standard calibration. Limits of detection (LoD) are listed in Tab. 4. The analytical error ranges within 10 % of the absolute concentration of the element. Detailed description of the measurement procedures were given by Flem et al. (2002) and Flem and Müller (2012). The analysed quartz crystals were examined by scanning electron microscope cathodoluminescence (SEM-CL) using a Centaurus BS Bialkali type CL detector prior to and after LA-ICP-MS analysis in order to relate the analyses to particular crystal growth zones, where growth zoning is developed, and to avoid the analysis of secondary quartz generations.

5. Results

5.1. Tourmaline composition

Tourmaline crystals, mostly 5–30 μm in size, are mostly unzoned (Fig. 3a, d). Bigger crystals, 50–150 μm across, show Fe enrichment from core to rim (Fig. 3c; Tab. 2). Microchemical analyses yielded Al_{TOT} from 5.568 to 6.613 a.p.f.u. and consequently the Z-site is assumed to be occupied by Al only or Al–Mg substitution is noted (Tab. 2), due to Al–Mg disorder (Tab. 2; Bloodaxe et al. 1999; Ertl et al. 2012). The variation in Y-site occupancy is expressed by $fm^Y = Fe^{2+}/(Fe^{2+} + Mg)$ ratio in the range 0.376–0.790 and varying amount of Al^Y (Fig. 4a–c, f; Tab. 2). Sodium is the main cation in the X-site (0.498–0.847 a.p.f.u; Tab. 2). The analysed tourmalines are poor in calcium (Ca/(Ca + Na) = 0.000–0.165; Figs 4a, 5), while K is slightly above detection level (Tab. 2). The calculated vacancies in the X-site are in the range 0.173–0.482 (Fig. 4b, d). Fluorine content is typically low (0.02–0.05 a.p.f.u.; Tab. 2).

However, tourmalines from the two breccia types differ in composition. Tourmalines from the T2 breccias are characterised by lower fm^Y ratios and plot consequently in the schorl–dravite–Mg-foitite compositional fields, whilst those from T1 breccias show higher fm^Y ratios and can be classified as schorl (Fig. 4a). On Na + K [a.p.f.u.] vs. V_X diagram (Fig. 4b), the first trend ($r^2 = 0.770$) describes the composition of tourmalines from T1 brecciated pegmatites, whilst the second ($r^2 = 0.923$) represents tourmalines from T2 breccias with a wider range of vacancy ratios. As a consequence, tourmalines from T2 breccias could be assigned to both the alkali-group and to a vacancy group, whilst those from T1 breccias plot exclusively in the alkali group field (Fig. 5). On Al_{TOT} [a.p.f.u.] vs. $Fe^{2+}{}_{TOT}$ [a.p.f.u.] diagram (Fig. 4c) T2 tourmalines fit also the common trend ($r^2 = 0.881$), while the T1 tourmalines do not form any linear correlation.

Tab. 2 Representative chemical compositions of tourmalines from T1 and T2 breccia zones. Site occupancy calculation is described in the text

sample	LoD	T1				T2			
component		#1	#2	#3	#4	#5	#6	#7	#8
SiO_2	0.03	35.25	36.14	35.63	35.15	36.18	36.49	37.22	37.07
TiO_2	0.02	0.00	0.00	0.76	0.71	0.20	0.15	0.11	0.12
Al_2O_3	0.01	33.46	30.02	31.08	31.47	30.10	30.41	34.64	34.14
B_2O_3 calc	–	10.56	10.38	10.34	10.35	10.50	10.38	10.73	10.67
FeO	0.05	11.20	13.54	11.60	11.35	11.10	10.30	7.89	8.12
MnO	0.06	0.09	0.00	0.14	0.14	0.00	0.00	0.06	0.08
MgO	0.01	4.69	4.50	4.43	4.64	6.41	5.74	5.25	5.27
CaO	0.02	0.22	0.56	0.72	0.73	0.00	0.02	0.11	0.14
Na_2O	0.01	1.98	2.21	2.02	2.06	2.64	2.42	1.78	1.62
K_2O	0.01	0.02	0.04	0.03	0.05	0.00	0.00	0.01	0.00
H_2O calc	–	3.62	3.57	3.52	3.50	3.60	3.58	3.70	3.66
F	0.02	0.04	0.03	0.11	0.14	0.04	0.00	0.00	0.05
Total		100.25	100.34	99.82	99.74	99.97	98.83	100.37	99.91
				T-sites					
Si		5.803	6.053	5.988	5.904	5.987	6.108	6.029	6.037
Al		0.197	0.000	0.012	0.096	0.013	0.000	0.000	0.000
Σ T		6.000	6.000	6.000	6.000	6.000	6.108	6.029	6.037
B		3.000	3.000	3.000	3.000	3.000	3.000	3.000	3.000
				Z-sites					
Al		6.000	5.926	6.000	6.000	5.857	5.999	6.000	6.000
Mg		0.000	0.074	0.000	0.000	0.143	0.001	0.000	0.000
				Y-sites					
Al		0.295	0.000	0.144	0.134	0.000	0.000	0.613	0.552
Ti		0.000	0.000	0.096	0.090	0.025	0.019	0.013	0.015
Fe^{+3}		0.308	0.518	0.326	0.319	0.307	0.577	0.214	0.221
Fe^{+2}		1.234	1.522	1.304	1.275	1.229	0.865	0.855	0.885
Mg		1.151	1.050	1.110	1.162	1.438	1.431	1.268	1.279
Mn		0.013	0.000	0.020	0.020	0.000	0.000	0.008	0.011
ΣY+Z		9.001	8.947	9.000	9.000	8.999	8.892	8.971	8.963
				X-sites					
Ca		0.039	0.100	0.130	0.131	0.000	0.004	0.019	0.024
Na		0.632	0.718	0.658	0.671	0.847	0.785	0.559	0.511
K		0.004	0.009	0.006	0.011	0.000	0.000	0.002	0.000
Xvac		0.325	0.173	0.206	0.187	0.153	0.211	0.420	0.465
				(W+V)-sites					
F		0.021	0.016	0.058	0.074	0.021	0.000	0.000	0.026
OH		3.979	3.984	3.942	3.926	3.979	4.000	4.000	3.974
$\#fm^Y$		0.516	0.592	0.540	0.523	0.461	0.500	0.376	0.408
Ca/(Ca+Na)		0.058	0.122	0.165	0.163	0.000	0.005	0.033	0.045

LoD – Limit of detection
$\#fm^Y = Fe^{2+}/(Fe^{2+} + Mg)$

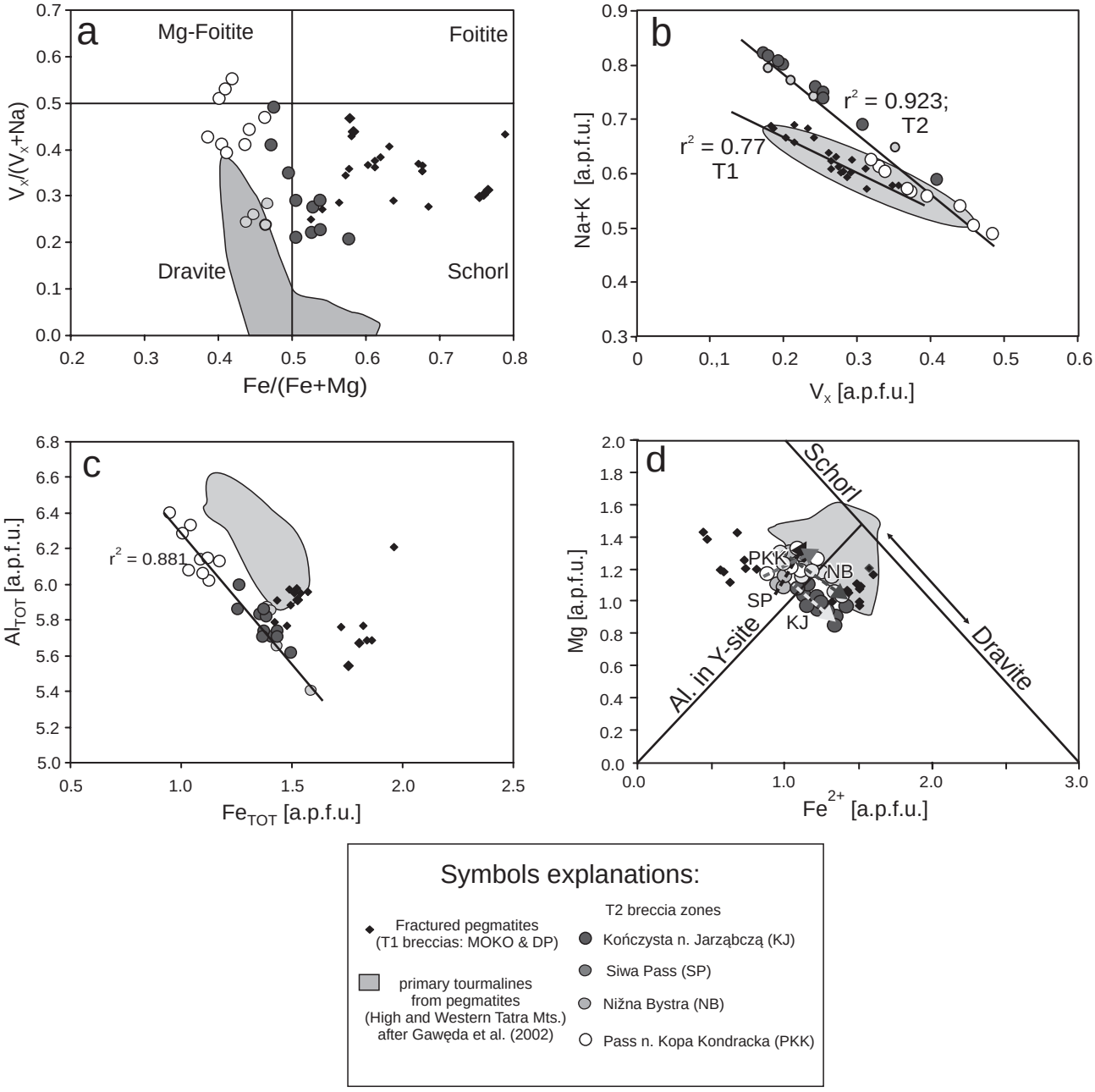

Fig. 4 Geochemical composition (presented in a.p.f.u.) of tourmalines according to Hawthorne and Henry (1999) from hydraulic breccias in the Tatra Mountains. The composition of tourmaline from pegmatites from the same area are used for comparison. **a** – Plot of Fe/(Fe + Mg) vs. vacancy ratio (V_x/V_x + Na); **b** – Plot of vacancy ratio (Vx) in X-position vs. Na + K; note two separate trends for T1 and T2 breccias; **c** – Plot of total Fe vs. total Al contents in tourmalines; a linear correlation with $r^2 = 0.881$ for T2 breccias is observed, while no correlation is seen for T1 breccia tourmalines; **d –** Plot of Fe^{2+} vs. Mg showing the interplay between schorl–dravite and Al in Y-site exchange in T1 and T2 tourmalines. Arrows show the local trends for the selected localities (see map in Fig. 1b and Appendix).

5.2. Mössbauer spectrometry of tourmaline and muscovite

In all tourmaline samples from the T2 breccias three doublets from Fe^{2+} were observed as well as two small doublets from Fe^{3+} (Fig. 6a; Tab. 3a). The latter forms *c.* 20 % of the total iron in PKK sample (Tab. 3a) and up to 38 % in the NB sample (Tab. 3b). One quadrupole assigned to charge-transfer/electron hoping ($Fe^{2.5+}$) is caused by the presence of both Fe^{3+} and Fe^{2+} in neighbouring Y structural positions, and accounts for *c.* 6.65 % of the total iron (Tab. 3a– b). The secondary tourmalines from T1 fractured pegmatites were difficult to separate from the primary types, so Mössbauer spectrometry was not carried out.

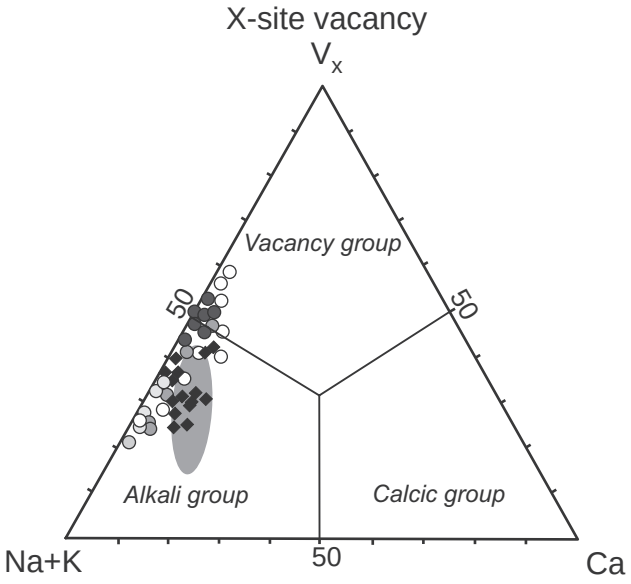

Fig. 5 Position of tourmalines from T1 and T2 breccias in Na + K – V_x – Ca classification diagram.

In the muscovite spectrum, two doublets from Fe^{2+} are observed, forming *c.* 37 % of the total iron in the muscovite, and three doublets from Fe^{3+} (Fig. 6b; Tab. 3b), all substituting Al in octahedral positions.

5.3. Quartz composition and geothermometry

After careful optical CL observations of thin sections, two representative samples of T1 and T2 breccias were selected for SEM–CL studies and trace-element analyses of quartz. Both samples have macroscopic textures typical of the localities. The examined quartz crystals do not show growth zoning in CL. However, both samples show a network of healed micro cracks seen in CL only (Fig. 7a–d). In the T1 sample the micro-cracks are healed with non-luminescent quartz connecting non-luminescent microdomains hosting fluid inclusions. These secondary structures are typical of plutonic quartz (Müller et al. 2010a and references therein). Occasionally, faint banding sub-parallel to grain boundaries is developed (Fig 7a). The T2 sample shows microcracks healed with brightly luminescent quartz and secondary microcrystalline feldspars (Fig. 7c–d). The secondary structures were avoided during LA-ICP-MS study.

Six LA-ICP-MS analyses were carried out on unaltered quartz domains of each sample (Tab. 4). Aluminium, which is the most common trace element in quartz (e.g. Götze et al. 2001; Müller et al. 2003), is low in both samples, with similar concentrations compared to published Al data from magmatic and hydrothermal quartz elsewhere (e.g. Jourdan et al. 2009; Müller et al. 2010b). The differences in Ti contents rank among the most conspicuous features distinguishing both samples

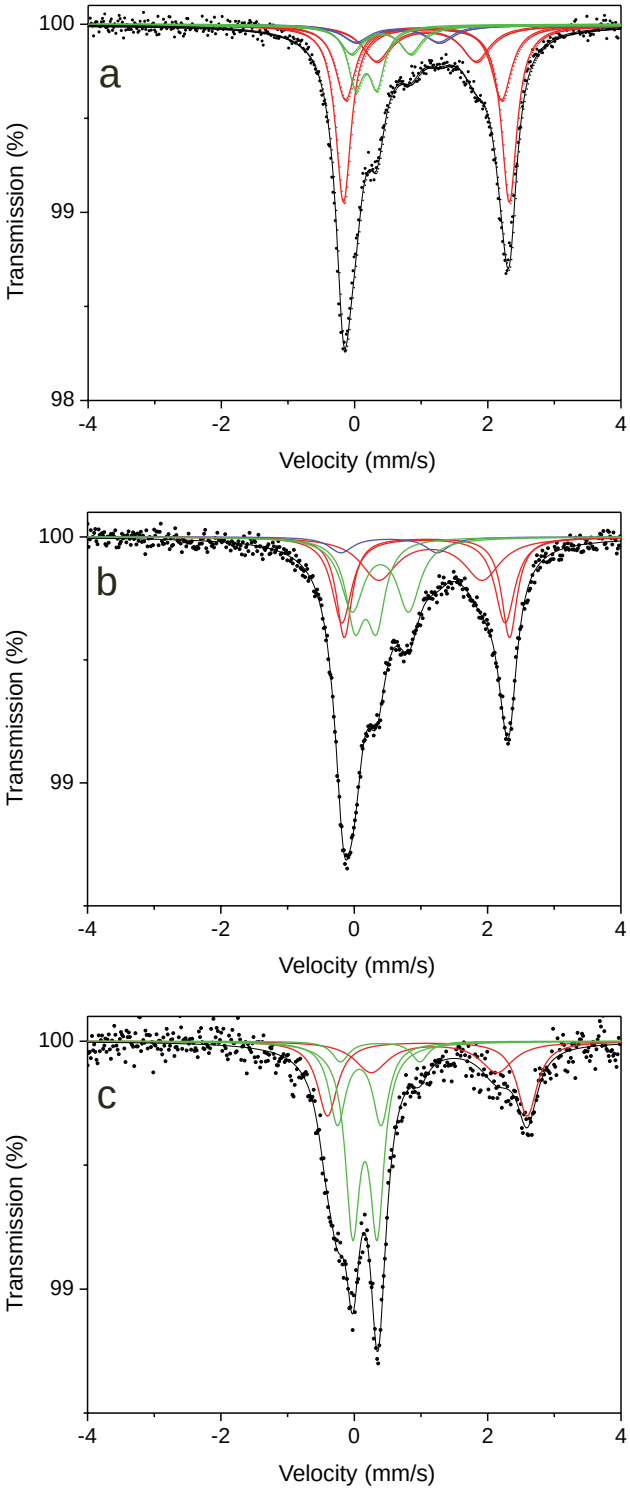

Fig. 6 Mössbauer spectra for the two selected tourmaline samples (**a** – PKK, **b** – NB) and one muscovite sample (**c** – SP) from T2 breccias. Spectroscopic parameters are given in Tab. 4a–c. Red lines mark doublets assigned to Fe^{2+}, green lines – Fe^{3+} and blue – $Fe^{2.5+}$ (charge transfer/electron hopping).

(Tab. 4). Quartz from the T1 breccia is characterised by a relatively high Ti content (17.1–32.1 ppm), whereas

Tab. 3 Hyperfine interaction parameters obtained from the Mössbauer spectra for the two selected tourmaline samples and one muscovite from T2 breccia

a) tourmaline from PKK sample

	IS (mm/s)	Qs (mm/s)	Γ (mm/s)	A (%)
Fe^{2+}	1.095 ± 0.005	2.490 ± 0.010	0.14 ± 0.01	37.83
	1.052 ± 0.015	2.342 ± 0.048	0.18 ± 0.01	20.63
	1.089 ± 0.016	1.494 ± 0.040	0.26 ± 0.04	14.19
$Fe^{2+}Fe^{3+}$ ED	0.660 ± 0.054	1.246 ± 0.076	0.25 ± 0.05	6.65
Fe^{3+}	0.410 ± 0.015	0.892 ± 0.048	0.20 ± 0.03	8.57
	0.191 ± 0.009	0.320 ± 0.012	0.14 ± 0.01	12.12

b) tourmaline from NB sample

	IS (mm/s)	Qs (mm/s)	Γ (mm/s)	A (%)
Fe^{2+}	1.106 ± 0.009	2.478 ± 0.016	0.14 ± 0.01	18.87
	1.055 ± 0.035	2.446 ± 0.054	0.18 ± 0.01	20.67
	1.160 ± 0.024	1.552 ± 0.040	0.33 ± 0.04	18.35
$Fe^{2+}Fe^{3+}$ ED	0.539 ± 0.151	1.446 ± 0.248	0.25 ± 0.05	6.65
Fe^{3+}	0.410 ± 0.015	0.846 ± 0.018	0.21 ± 0.03	19.90
	0.188 ± 0.008	0.320 ± 0.012	0.16 ± 0.01	17.67

c) muscovite from SP sample

	IS (mm/s)	Qs (mm/s)	Γ (mm/s)	A (%)
Fe^{2+}	1.113 ± 0.005	2.994 ± 0.006	0.18 ± 0.01	22.10
	1.214 ± 0.016	1.881 ± 0.044	0.30 ± 0.02	15.06
	0.405 ± 0.031	1.190 ± 0.043	0.15 ± 0.01	5.01
Fe^{3+}	0.176 ± 0.002	0.336 ± 0.004	0.13 ± 0.01	38.08
	0.092 ± 0.002	0.654 ± 0.012	0.15 ± 0.01	19.77

See Fig. 2d–e
IS – isomer shift, QS – quadrupole splitting, Γ – half-intensity width, A – per-cent contribution

quartz from the T2 breccia is poorer in Ti (2.2 and 3.7 ppm). Lithium, B and K are relatively high compared to quartz composition described from other environments (e.g. Müller and Koch-Müller 2009).

The Ti concentrations have been used for calculation of the quartz crystallization temperature, applying the Ti-in-quartz geothermometer of Wark and Watson (2006). Quartz from the T1 sample crystallized between 572 and 627 ºC, supporting its magmatic origin suggested already by the secondary CL structures. Quartz in the T2 sample gives temperatures of 465–430 ºC, indicating hydrothermal and/or magmatic–hydrothermal transition regimes.

5.4. *Molybdenite characteristics and dating*

Molybdenite is observed as single isolated blades (<3 mm) or a small aggregate of crystals (6 mm in diameter; Fig. 2c) in brecciated pegmatite (T1) within a coarse-grained leucocratic porphyritic granite. Minute molybdenite flakes occur within quartz and tourmaline matrix sealing brecciated K-feldspar, albite and Tur_1 tourmaline crystals both inside T1 and T2 breccias. Molybdenite post-dated the primary tourmaline and was contemporaneous with the secondary mineralization.

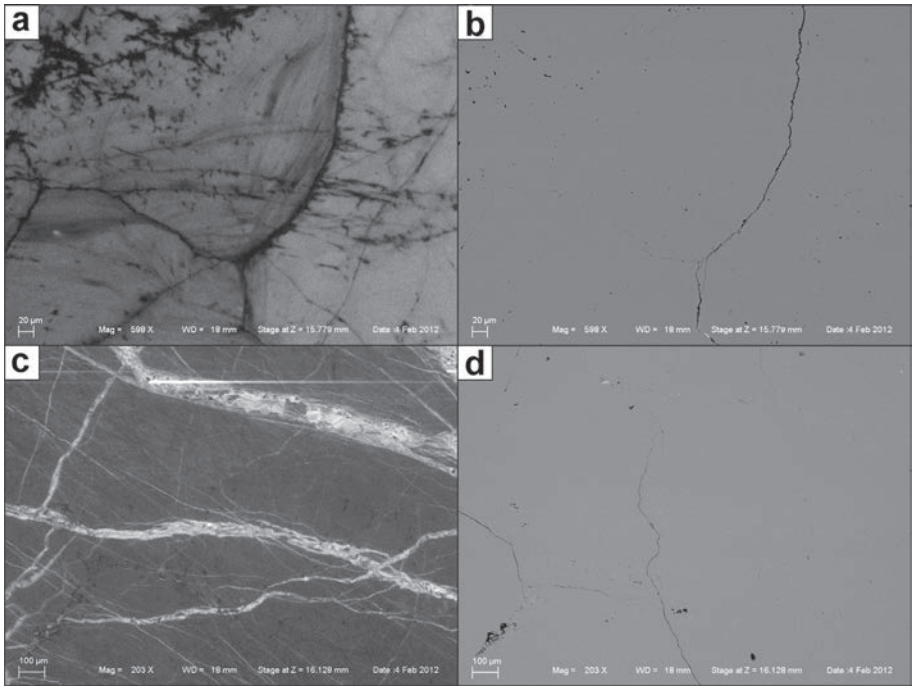

Fig. 7 Cathodoluminescence (CL) and BSE images of quartz from tourmaline-rich breccias. **a –** CL image of quartz from T1 breccia (MOKO sample), displaying faint banding sub-parallel to the grain boundaries; **b –** BSE image of (a) showing the healed micro-cracks; **c –** CL image of quartz from T2 breccia cut by secondary micro cracks healed by bright luminescent quartz; **d –** BSE image of (c) with healed micro-cracks in quartz.

Tab. 4 Trace-element contents of quartz associated with tourmaline, analysed by LA-ICP-MS (ppm)

sample	LoD	T1						T2					
element		#1	#2	#3	#4	#5	#6	#1	#2	#3	#4	#5	#6
Li	0.07	10.62	8.29	9.80	7.49	8.71	8.96	7.53	7.70	8.74	4.11	7.27	3.32
Be	0.04	0.10	<0.04	<0.04	<0.04	0.06	<0.04	<0.04	<0.04	<0.04	0.10	<0.04	<0.04
B	1.04	1.63	1.51	2.04	1.34	2.64	3.09	1.64	1.78	1.80	1.47	1.48	1.74
Mn	0.11	0.15	0.16	0.53	<0.11	0.33	0.29	1.53	0.59	0.72	0.41	0.35	0.90
Ge	0.06	1.03	1.01	0.80	1.11	1.21	0.82	0.95	0.95	1.07	1.25	1.28	1.22
Rb	0.02	0.02	0.00	0.14	0.00	0.09	<0.02	0.09	0.04	0.09	0.03	0.03	0.06
Sr	0.01	0.97	0.32	1.30	0.03	5.17	1.64	3.83	2.73	7.11	3.97	3.28	3.12
Sb	0.03	0.40	0.61	0.47	0.48	0.95	0.95	0.01	0.05	0.09	0.08	0.12	0.11
Al	6.60	35.52	37.63	51.30	45.76	38.95	51.58	37.32	50.59	40.55	48.75	75.32	33.77
P	2.50	<2.50	<2.50	<2.50	<2.50	<2.50	<2.50	<2.50	<2.50	<2.50	<2.50	<2.50	<2.50
K	14.50	<14.50	<14.50	16.69	<14.50	<14.50	<14.50	19.43	19.71	19.53	36.07	20.60	<14.50
Ti	1.50	25.00	24.41	32.06	23.54	17.08	17.88	3.70	3.39	2.75	2.27	3.91	2.48
Fe	1.40	<1.40	<1.40	<1.40	1.52	<1.40	<1.40	<1.40	<1.40	1.46	3.02	19.86	<1.40
Zn	1.00	1.21	<1.00	<1.00	<1.00	<1.00	<1.00	<1.00	<1.00	<1.00	<1.00	1.45	1.10
T_{min} [°C]		594.6	592.5	616.9	589.3	562.5	566.2	454.6	449.2	436.7	425.7	458.0	430.7
T_{max} [°C]		613.9	611.8	636.9	608.5	580.9	584.7	469.8	464.2	451.3	440.0	473.2	445.2
T_{mean} [°C]		604.2	602.1	626.9	598.9	571.6	575.4	462.2	456.6	444.0	432.9	465.5	437.9

LoD – Limit of detection

The crystallization temperatures of quartz T_{min}, T_{max}, T_{mean} were calculated applying the Ti-in-geothermometer of Wark and Watson (2006).

The analyzed molybdenite sample has a Re concentration of 16.58 ± 0.01 ppm, and a radiogenic ^{187}Os concentration of 61.04 ± 5 ppb. Using a double Os spike, the common Os was measured and is essentially zero. These data provide a ^{187}Re–^{187}Os model age of 350 ± 1 Ma, indicating a period of molybdenite crystallization in Carboniferous, Early Mississippian (Tournaisian) times. The sulphur isotopic composition, expressed as $\delta^{34}S_{CDT}$, equals +2.35‰.

6. Discussion

6.1. Crystallization conditions

Post-magmatic mineralization, both boron- and sulphide rich, in the Tatra granite and its metamorphic envelope is not common but occurs locally in some pegmatites (Gawęda et al. 2002) and quartz–tourmaline–feldspar pockets (Gawęda and Szopa 2011). The presence of breccias, cemented by tourmaline and quartz, suggests that boron, along with water, dominated in the exsolved fluid phase which, however, did not contribute to the development of pegmatites. As pegmatite-like lenses without tourmaline crystals show no brecciation, possibly boron alone stimulated the process.

In T1 breccias, the metasomatic replacement of brecciated K-feldspars and overgrowth of the pegmatitic Tur_1 tourmalines by micro-crystalline Tur_2 varieties (Fig. 3a–b) suggest rather redistribution of elements during metasomatic alteration and inheritance of tourmaline (Tur_2) composition from primary pegmatitic tourmalines. The high Ti and Fe contents in these tourmaline crystals, together with the lack of biotite in both pegmatites and breccias, could have resulted from the recycling of magmatic biotite components, mobilized by the boron-rich fluid. This could be the cause of the observed lack of any clear compositional trend in Al_{TOT} vs. Fe_{TOT} and Mg vs. Fe^{2+} diagrams (Fig. 4c–d) and the trend inherited from primary tourmalines on the Na + K vs. Vx diagram (Fig. 4b).

The microcrystalline to fine-grained nature of quartz–tourmaline matrix in the T2 breccias reflects a relatively rapid crystallization from the fluid. The high vacancy ratio (Vx) in the X-sites (Tab. 2; Fig. 4a–b), together with the scarcity of crystal zonation (Fig. 3c–d), could be also a result of rapid crystallization (Novák et al. 2004), whilst the coexistence of tourmaline with ore minerals suggests fluid boiling (Slack and Trumbull 2011). However, the scarce zoned tourmaline crystals, showing a Fe increase towards the margins (Fig. 3c) might be a signature of limited Fe–Mg fractionation during crystallization of the matrix in T2 breccias. As in hydraulic breccias the composition of tourmaline is buffered by the fluid phase, such that the tourmaline composition could be a monitor of fluid modification (Slack and Trumbull 2011). Observations at selected localities of the T2 breccias point to the growing vacancy ratio and Al content from the margin to the central part of the veins, which is consistent with the linear compositional trends (Fig. 4b–d). The substitution mechanisms in both types seem to be a mixture of Al in Y-site and schorl–dravite exchange. In some localities the predominance of the schorl–dravite exchange or Al in Y-site can be seen (Fig. 4d).

The results of the Ti-in-quartz geothermometry suggest a temperature range of 627–572 ºC for T1 and 465–430 ºC for T2 (Tab. 4). The former range is typical of late-magmatic conditions of fracturing, i. e. crystallization in pegmatites, whilst the latter suggests late pegmatitic–hydrothermal conditions, comparable with the cooling temperatures obtained from ternary feldspar geothermometry (Gawęda and Szopa 2011). Calibration of the pressure range using the Massonne and Schreyer (1987) method for the zoned phengitic muscovite (Fig. 3e; Tab. 1) suggests that in pegmatitic segregations the exsolved volatile components could have locally built up a pressure of 6.0 to 7.5 kbar (Fig. 8). Given that the calibrated pressure for different parts of the Tatra granite Pluton was 4.5–6 kbar (Ludhová and Janák 1999; Gawęda et al. 2005; Gawęda 2009; Burda et al. 2011; Gawęda and Szopa 2011), it could have exceeded the lithostatic pressure, favouring hydrofracturing of the internal pegmatitic components as well as of the host granite. Crystallization inside the distant fracture zones (T2), calibrated for the unzoned, syntectonic muscovite (Fig. 3f), coexisting with tourmaline, took place under lower pressure conditions (2.5–1.5 kbar; Fig. 8).

6.2. Fluid characteristics and age

The presence of sulphides, especially the spectacular molybdenite, and relatively high Fe^{3+} content (20–38 %; Tab. 3a–b) in tourmalines suggest that the precipitation occurred from a superheated, rather oxidized fluid (Yavuz et al. 1999; Slack and Trumbull 2011). The high fO_2 of the fluid is supported by the predominance of Fe^{3+} in the muscovite associated with tourmaline (Tab. 3c). The positive $\delta^{34}S$ value of the molybdenite is typical of granite-related sulphide mineralization (Rollinson 1993) and is similar to the sulphur isotopic composition of hydrothermal tetrahedrites from the Tatra Mountains ($\delta^{34}S_{CDT}$ = +1.91 to +2.95; Gawęda et al. 2007). The 350 ± 1 Ma model age of molybdenite from the brecciated pegmatite fits within error the whole-rock Rb–Sr isochron age of pegmatites from the same area (345 ± 9.5 Ma; Gawęda 1995), and the U–Pb zircon ages of the host granites (360–340 Ma; Poller et al. 2000; Gawęda 2008; Burda et al. 2013). Molybdenite age presented here supports also the U–Pb dating of the magmatic activity in the Inner Western Carpathians which was attributed to the prolonged subduction and final plate collision and closure of the Rheic Ocean (Gawęda and Golonka 2011; Broska et al. 2013; Burda et al. 2013 and references therein). This is the oldest recorded molybdenite mineralization in the Inner Carpathians (cf. Kohút and Stein 2005; Kohút et al. 2013).

6.3. Possible scenario of formation of the fracture zones

In contrast to the classical pegmatites, locally with tourmaline (Gawęda et al. 2002), volatile components exsolved from the slowly cooling granitoid body, originally rich in water (5–6 % H_2O in melt) were concentrated into pockets and lenses, screened by the impermeable bases of the magmatic layers, rich in sheet silicates and opaque minerals (Gawęda and Szopa 2011).

During crystallization they formed pegmatite-like bodies, locally rich in tourmaline (Fig. 9 a). The internal pressure in such fluid-rich pockets could have locally exceeded that of the overburden rocks, favouring the escape of the superheated fluid by hydraulic fracturing. The resulting fracture zones could have provided paths for fluid migration and rapid crystallization as the pressure and temperature dropped (Figs 8, 9b; see Derham and Feely 1988). Where the fluid could not escape, the pegmatite-like pockets show internal brecciation and metasomatic replacement of K-feldspars by tourmaline, due to the overpressure and high B, Al and H_2O contents in the fluid phase.

Thus in this simplified model, the key role for the formation of channelized fluid flow and hydraulic breccia formation close to the magmatic

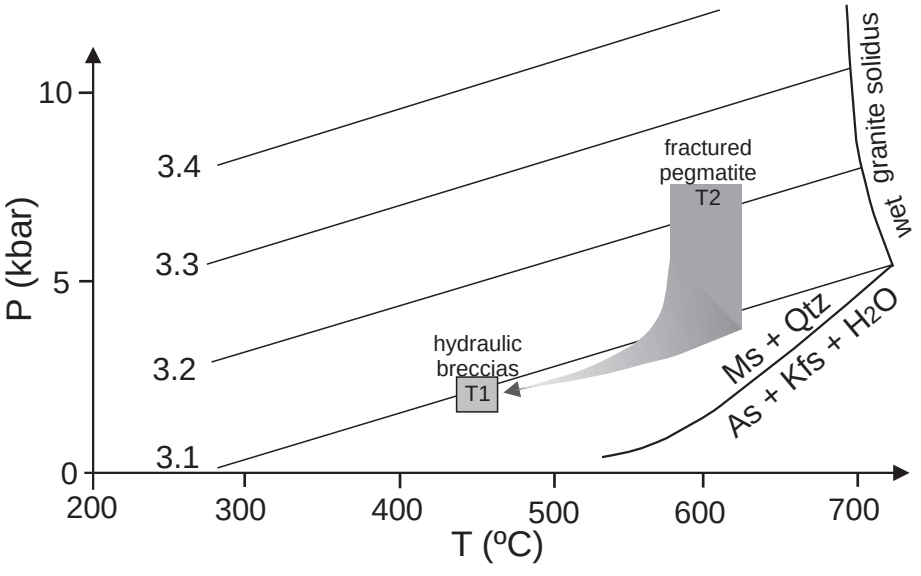

Fig. 8 An illustration of the change in P–T conditions of formation for the two types of breccias. Silica contents of phengite isopleths are from Massonne and Schreyer (1987).

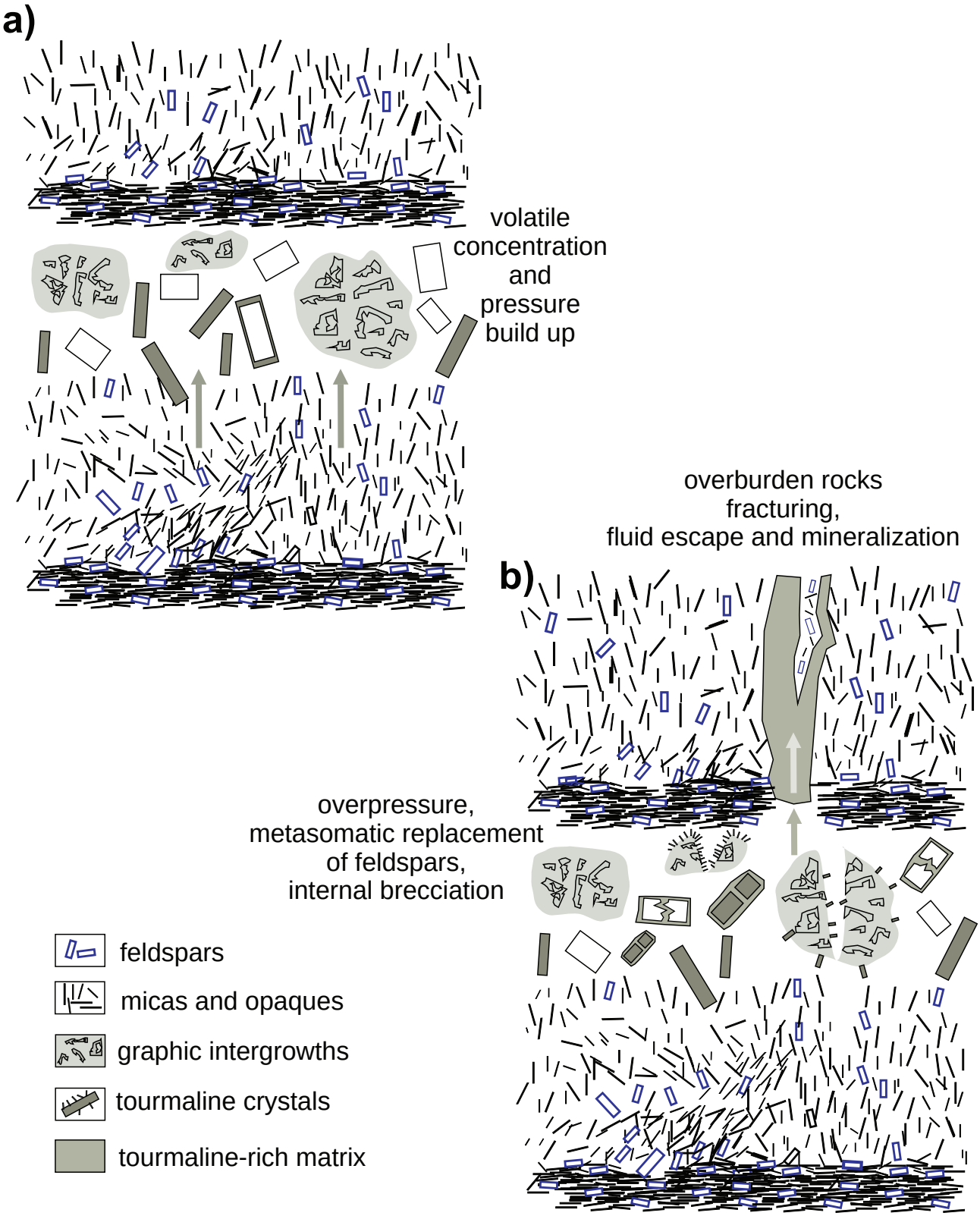

Fig. 9 A model of hydraulic breccia formation in relation to the magmatic layering in the host granite. **a –** The segregation of exsolved volatiles in the upper part of the slowly cooling layer, crystallization of pegmatite-like pockets with tourmaline crystals and local graphic intergrowths of K-feldspar with quartz; growing pressure locally causes metasomatic replacement of feldspars by tourmaline. **b –** Overpressure of the fluid leads to the internal fracturing and then fracturing of the overburden rocks; escaping fluid precipitates microcrystalline tourmalines both on the brecciated minerals of the pegmatite-like body and inside the fracture due to dropping pressure and temperature.

source is attributed to the fluid circulation and local overpressure.

7. Conclusions

1. The formation of tourmaline-rich breccias should be linked to the internal structure of the granitoid intrusion. The layered character of the granitoid body is thought to have restricted the exsolved fluid migration and promoted the formation of pegmatite-like pockets on the top of the individual graded layers. Local overpressure presumably caused metasomatic alteration, brecciation and finally the escape of the boron-rich fluid.
2. The precipitation of the tourmaline–quartz mineralization in breccias could have taken place from superheated, possibly boiling oxidized fluid, exsolved from the cooling granitoid magma. The age of brecciation was constrained at 350 ± 1 Ma by Re–Os molybdenite dating.
3. Brecciation and metasomatic replacement in T1 took place under subsolidus conditions (6–7.5 kbar; 570–630 ºC), whilst rapid crystallization in T2 breccia veins occurred from cooling fluids at decreasing pressure and temperature (1.5–2.5 kbar, 430–465 ºC).
4. The differences in P–T conditions correlate well with two compositional trends found in tourmaline. Large variations in vacancy ratios in T2 tourmalines were possibly caused by rapid crystallization leading also to disorder in Al–Fe^{3+}–Mg substitution in Z-sites and Al exchange in Y-sites. The composition of T1 tourmalines might be at least partly inherited from the primary mineral phases (biotite or primary tourmaline).

Acknowledgements. This work was financially supported by Polish Ministry of Science and Higher Education grant No. N 307 027837 given to AG and CSR grant No 525 393739 to SM. We are grateful to Geological Survey of Norway, which supported the LA-ICP-MS quartz analyses. Piotr Dzierżanowski and Lidia Jeżak are thanked for their help during electron microprobe analyses. Careful reviews by Adam Pieczka, David London and Pavel Uher, as well as editorial comments of Vojtěch Janoušek significantly improved the manuscript. Ray Macdonald (Warsaw University, Poland) is thanked for final correction of the English. Prof. van Hinsberg is greatly acknowledged for sending the necessary literature.

References

Bloodaxe ES, Hughes JM, Dyar MD, Grew ES, Guidotti CV (1999) Linking structure and chemistry in the schorl–dravite series. Amer Miner 84: 922–928

Broska I, Petrík I, Be`eri-Shlevin Y, Majka J, Bezák V (2013) Devonian/Mississippian I-type granitoids in the Western Carpathians: a subduction-related hybrid magmatism. Lithos 162–163: 27–36

Burchart J (1972) Fission-track age determination of accessory apatite from the Tatra Mountains, Poland. Earth Planet Sci Lett 15: 418–422

Burda J, Gawęda A (2009) Shear-influenced partial melting in the Western Tatra metamorphic complex: geochemistry and geochronology. Lithos 110: 373–385

Burda J, Gawęda A, Klötzli U (2011) Magma hybridization event in the Western Tatra Mts. granitoid intrusion (S-Poland, Western Carpathians). Mineral Petrol 103: 19–36

Burda J, Gawęda A, Klötzli U (2013) U–Pb zircon age of the youngest magmatic activity in the High Tatra granite. Geochronometria 40: 134–144

Buriánek D, Novák M (2007) Compositional evolution and substitutions in disseminated and nodular tourmaline from leucocratic granites: examples from the Bohemian Massif, Czech Republic. Lithos 95: 148–164

Derham JM, Feely M (1988) A K-feldspar breccia from Mo–Cu stockwork deposit in the Galway granite, west of Ireland. J Geol Soc, London 145: 661–667

Dini A, Mazzarini F, Musumeci G, Rocchi S (2008) Multiple hydrofracturing by boron-rich fluids in the Late Miocene contact aureole of eastern Elba Island (Tuscany, Italy). Terra Nova 20: 318–326

Ertl A, Kolitsch U, Dyar MD, Hughes JM, Rossman GR, Pieczka A, Henry DJ, Pezzotta F, Provatke S, Lengauer CL, Körner W, Brandtstätter F, Francis CA, Prem M, Tillmanns E (2012) Limitations of Fe^{2+} and Mn^{2+} site occupancy in tourmaline: evidence from Fe^{2+}- and Mn^{2+}-rich tourmaline. Amer Miner 97: 1402–1416

Feely M, Selby D, Hunt J, Conliffe J (2010) Long-lived granite-related molybdenite mineralization at Connemara, western Irish Caledonides. Geol Mag 147: 886–894

Flem B, Müller A (2012) In situ analysis of trace elements in quartz using laser ablation inductively coupled mass spectrometry. In: Götze J, Möckel R (eds) Quartz Deposits – Mineralogy and Analytics. Springer Verlag, Berlin, pp 219–236

Flem B, Larsen RB, Grimstvedt A, Masfeld J (2002) In situ analysis of trace elements in quartz by using laser ablation inductively coupled plasma mass spectrometry. Chem Geol 182: 237–247

Fuchs Y, Lagache M, Linares J (1998) Fe-tourmaline synthesis under different T and fO_2 conditions. Amer Miner 83: 525–534

Gawęda A (1995) Geochemistry and Rb/Sr isochron age of pegmatites from the Western Tatra Mts. (S-Poland). Geol Carpath 46: 95–99

Gawęda A (2008) Apatite-rich enclave in the High Tatra granite, Western Carpathians: petrological and geochronological study. Geol Carpath 59: 295–306

Gawęda A (2009) Enclaves in the High Tatra Granite. University of Silesia Publishing House, Monograph Series, Katowice, pp 1–180 (in Polish, English abstract)

Gawęda A, Golonka J (2011) Variscan plate dynamics in the Circum-Carpathians area. Geodin Acta 23: 141–155

Gawęda A, Szopa K (2011) The origin of magmatic layering in the High Tatra granite, Central Western Carpathians – implications for the formation of granitoid plutons. Earth Environ Sci Trans R Soc Edinb 103: 129–144

Gawęda A, Pieczka A, Kraczka J (2002) Tourmalines from the Western Tatra Mountains (Central Western Carpathians): their characteristics and petrogenetic importance. Eur J Mineral 14: 943–955

Gawęda A, Doniecki T, Burda J, Kohút M (2005) The petrogenesis of quartz-diorites from the Tatra Mountains (Central Western Carpathians): an example of magma hybridisation. Neu Jb Mineral, Abh 181: 95–109

Gawęda A, Jędrysek MO, Zieliński G (2007) Polystage mineralization in tectonic zones in the Tatra Mountains, Western Carpathians. In: Kozłowski A, Wiszniewska J (eds) Granitoids in Poland. Archiwum Mineralogiczne Monograph 1: 341–353

Götze J, Plötze M, Habermann D (2001) Origin, spectra characteristics and practical applications of the cathodoluminescence (CL) of quartz – a review. Mineral Petrol 71: 225–250.

Grabowski J, Gawęda A (1999) Preliminary paleomagnetic study of the High Tatra granites, Central Western Carpathians, Poland. Geol Q 43: 263–276

Hawthorne FC, MacDonald DJ, Burns PC (1993) Reassignment of cation site-occupancies in tourmaline: Al–Mg disorder in the crystal structure of dravite. Amer Miner 78: 265–270

Hawthorne FJ, Henry DJ (1999) Classification of minerals of the tourmaline group. Eur J Mineral 11: 201–216

Henry DJ, Guidotti CV (1985) Tourmaline as a petrogenetic indicator mineral: an example from the staurolite-grade metapelites from NW Maine. Amer Miner 70: 1–15

Henry DJ, Novák M, Hawthorne FC, Ertl A, Dutrow BL, Uher P, Pezzotta F (2011) Nomenclature of the tourmaline-super-group minerals. Amer Miner 96: 895–913

Jourdan A-L, Vennemann TW, Mullis J, Ramseyer K, Spiers CJ (2009) Evidence of growth and sector zoning in hydrothermal quartz from Alpine veins. Eur J Mineral 21: 219–231.

Kohút M, Janák M (1994) Granitoids of the Tatra Mts., Western Carpathians: field relations and petrogenetic implications. Geol Carpath 45: 301–311

Kohút M, Sherlock S (2003) Laser microprobe ^{40}Ar–^{39}Ar analysis of pseudotachylyte and host-rocks from the Tatra Mountains, Slovakia: evidence for late Palaeogene seismic/tectonic activity. Terra Nova 15: 417–424

Kohút M, Stein H (2005) Re–Os molybdenite dating of granite-related Sn–W–Mo mineralization at Hnilec, Gemeric Superunit, Slovakia. Mineral Petrol 85: 117–129

Kohút M, Stein H, Uher P, Zimmerman A, Hraško L (2013) Re–Os and U–Th–Pb dating of the Rochovce granite and its mineralization (Western Carpathians, Slovakia). Geol Carpath 64: 71–79

London D (1996) Granitic pegmatites. Trans Roy Soc Edinb, Earth Sci 87: 305–319

London D (2009) The origin of primary textures in granitic pegmatites. Canad Mineral 47: 697–724

Ludhová L, Janák M (1999) Decompression and exhumation of Variscan orogenic root in the Tatra Mountains, Western Carpathians: evidence from high-grade metapelites. Geol Carpath, 50: 120–122

MacDonald DJ, Hawthorne FC, Grice JD (1993) Foitite, $\square[Fe^{2+}(Al,Fe^{3+})]Al_6Si_6O_{18}(BO_3)_3(OH)_4$, a new alkali-deficient tourmaline: description and crystal structure. Amer Miner 78:1299–1303

Massonne HJ, Schreyer W (1987) Phengite geobarometry based on the limited assemblage with K-feldspar, phlogopite and quartz. Contrib Mineral Petrol 96: 212–224

Müller A, Halls C (2005) Rutile – the tin–tungsten host in the intrusive tourmaline breccia at Wheal Remfry, SW England. In: Jingwen M, Bierlein FP (eds) Mineral Deposit Research: Meeting the Global Challenge, pp 441–444

Müller A, Koch-Müller M (2009) Hydrogen speciation and trace element content of igneous, hydrothermal and metamorphic quartz from Norway. Mineral Mag 73: 569–583

Müller A, Wiedenbeck M, van der Kerkhof AM, Kronz A, Simon K (2003) Trace elements in quartz – a combined electron microprobe, secondary ion mass spectrometry, laser ablation ICP-MS, and cathodoluminescence study. Eur J Mineral 15: 747–763

Müller A, Williamson BJ, Smith M (2005) Origin of quartz cores in tourmaline from Roche Rock, SW England. Mineral Mag 69: 381–401

Müller A, Seltmann R, Halls C, Siebel W, Dulski P, Jeffries T, Spratt J, Kronz A (2006) The magmatic evolution of the Land`s End Pluton, Cornwall, and associated pre-enrichment of metals. Ore Geol Rev 28: 329–367

Müller A, Herrington R, Armstrong R, Seltmann R, Kirwin DJ, Stenina NG, Kronz A (2010a) Trace elements and cathodoluminescence of quartz in stockwork veins of Mongolian porphyry-style deposits. Miner Depos 45: 707–727

Müller A, van den Kerkhof AM, Behr H-J, Kronz A, Koch-Müller M (2010b) The evolution of late-Hercynian granites and rhyolites documented by quartz – a review. In: Geological Society of America Special Papers 472: 185–204

Novák M, Povondra P, Selway JB (2004) Schorl–oxyschorl to dravite–oxy-dravite tourmaline from granitic

pegmatites; examples from the Moldanubicum, Czech Republic. Eur J Mineral 16: 323–333

Pawlica W (1913) Pegmatites of the Polish Tatra Mts. and their magmatogenic relations. Rozpr Acad Um Sci ser A Kraków pp 3–25 (in Polish)

Pieczka A, Kraczka J (2004) Oxidized tourmalines – a combined chemical, XRD and Mössbauer study. Eur J Mineral 16: 309–321

Pollard PJ, Pichavant M, Charoy B (1987) Contrasting evolution of fluorine- and boron-rich systems. Miner Depos 22: 315–321

Poller U, Janák M, Kohút M, Todt W (2000) Early Variscan magmatism in the Western Carpathians: U–Pb zircon data from granitoids and orthogneisses of the Tatra Mountains, Slovakia. Int J Earth Sci 89: 336–349

Poller U, Todt W (2000) U–Pb single zircon data of granitoids from the High Tatra Mountains (Slovakia): implications for the geodynamic evolution. Tr Roy Soc Edinb, Earth Sci 91: 235–234

Rollinson HR (1993) Using Geochemical Data: Evaluation, Presentation, Interpretation. Longman, London, pp 1–352

Sillitoe RH, Sawkins FJ (1971) Geologic, mineralogical and fluid inclusion studies relating to the origin of copper-bearing tourmaline breccia pipes, Chile. Econ Geol 66: 1028–1041

Skewes MA, Holmgren C, Stern CR (2003) The Donoso copper-rich, tourmaline-bearing breccia pipe in central Chile: petrologic, fluid inclusion and stable isotope evidence for an origin from magmatic fluids. Miner Depos 38: 2–21

Slack JF, Trumbull RB (2011) Tourmaline as a recorder of ore-forming processes. Elements 7: 321–326

Stein H (2006) Low-rhenium molybdenite by metamorphism in northern Sweden: recognition, genesis, and global implications. Lithos 87: 300–327

Stein H, Markey RJ, Morgan JW, Hannah JL, Scherstén A (2001) The remarkable Re–Os chronometer in molybdenite: how and why it works. Terra Nova 13: 479–486

Szopa K, Gawęda A, Müller A, Sikorska M (in print) The petrogenesis of granitoid rocks unusually rich in apatite in the Western Tatra Mts. (S-Poland, Western Carpathians). Mineral Petrol. doi: 10.1007/s00710–012–0262–2

van Hinsberg VJ, Henry DJ, Marschall HR (2011a) Tourmaline: an ideal indicator of its host environment. Canad Mineral 49: 1–16

van Hinsberg VJ, Henry DJ, Dutrow BL (2011b) Tourmaline as a petrologic forensic mineral: a unique recorder of its geologic past. Elements 7: 327–332

von Goerne G, Franz G, van Hinsberg V (2011) Experimental determination of Na–Ca distribution between tourmaline and fluid in the system $CaO–Na_2O–MgO–Al_2O_3–SiO_2–B_2O_3–H_2O$. Canad Mineral 49: 137–152

Wątocki W (1950) Ore veins in the Ornak zone in the Western Tatra Mts. Rocznik PTG 20 (1–2): 11–60 (in Polish)

Wark DA, Watson EB (2006) TitaniQ: a titanium-in-quartz geothermometer. Contrib Mineral Petrol 152: 743–754

Williamson BJ, Spratt J, Adams JT, Tindle AG, Stanley CT (2000) Geochemical constraints from zoned hydrothermal tourmalines on fluid evolution and Sn mineralization: an example from fault breccias at Roche, SW England. J Petrol 41: 1439–1453

Yavuz F, İskenderoğlu A, Jiang S-Y (1999) Tourmaline compositions from the Salikvan porphyry Cu–Mo deposit and vicinity, northeastern Turkey. Canad Mineral 37: 1007–1023